THE JOURNAL OF PHYSICAL CHEMISTRY C

ARTICLE

pubs.acs.org/JPCC

Electronic Structure and Photoluminescence Origin of Single-Crystalline Germanium Oxide Nanowires with Green Light Emission

Mingfa Peng,[†] Yang Li,[†] Jing Gao,[†] Duo Zhang,[†] Zheng Jiang,[*,‡] and Xuhui Sun[*,†]

[†]Institute of Functional Nano and Soft Materials (FUNSOM) and Jiangsu Key Laboratory for Carbon-based Functional Materials and Devices, Soochow University, Suzhou, Jiangsu 215123, P. R. China

[‡]Shanghai Synchrotron Radiation Facility, Shanghai Institute of Applied Physics, Chinese Academy of Sciences, Shanghai 201204, P. R. China

ABSTRACT: High-quality single-crystalline germanium oxide nanowires (GeONWs) have been synthesized by a thermal evaporation method under a vapor−liquid−solid mechanism. The morphology and nanostructure of the as-synthesized GeONWs were characterized by scanning electron microscopy (SEM), X-ray diffraction (XRD), and transmission electron microscopy (TEM). Energy-dispersive X-ray spectroscopy (EDS) and X-ray photoelectron spectroscopy (XPS) of the GeONWs showed the presence of substoichiometric oxygen. The electronic structure and local structure of GeONWs were also investigated by X-ray absorption fine structure (XAFS), which showed disorder and degradation of long-range order in the nanowires due to the nanosize in one-dimension and oxygen vacancies in the nanowires. Synchrotron-radiation-based X-ray-excited optical luminescence (XEOL) from GeONWs exhibits strong green light at 2.3 eV (540 nm), which corresponds to the photoluminescence (PL) spectrum of the individual GeONWs excited by laser. The strong emission is attributed to oxygen-related defect states in oxygen vacancies confirmed by X-ray absorption near-edge structure (XANES) and XEOL.

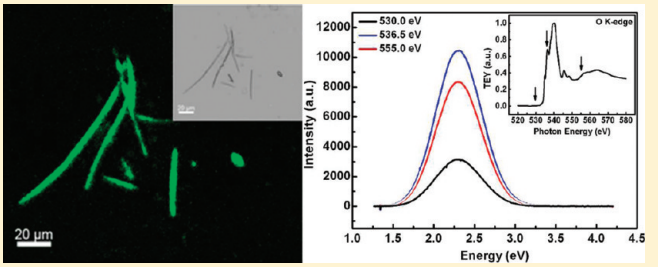

INTRODUCTION

Germanium dioxide (GeO_2) has attracted much attention because of its unique electronic and optical properties (such as high refractive index to visible light and dielectric oxide with visible light photoluminescence)[1,2] with potential applications in optoelectronics, such as optical wave guides for integrated optical systems and nanoconnections in optical devices and systems,[3,4] especially with one-dimensional nanowires.[5,6] GeO_2 also has a higher band gap energy (5 eV) than other transparent conductive oxide materials, which makes it attractive as a host for optical impurities to develop luminescent devices, from the ultraviolet-blue to the near-infrared range.[7] In general, GeO_2 nanocrystals emit violet and blue photoluminescence (PL) because of oxygen vacancies or other surface defects.[8,9] The types of oxygen defects can affect the luminescence properties.[10,11] However, information on the origin of PL in GeO_2 nanowires and the relative electronic and local structures, which is critical to optical applications of GeO_2 nanowires, is not clear yet.

In this work, high-quality single-crystalline germanium oxide nanowires (GeONWs) have been synthesized by a simple thermal evaporation method under a vapor−liquid−solid (VLS) mechanism. The morphology, nanostructure, and composition of the as-synthesized GeONWs were characterized by scanning electron microscopy (SEM), X-ray diffraction (XRD), transmission electron microscopy (TEM) combined with energy-dispersive X-ray spectroscopy (EDS), and X-ray photoelectron spectroscopy (XPS). The local structure and electric structure of GeONWs were studied by X-ray absorption fine structure (XAFS) including X-ray absorption near-edge structure (XANES) and extended X-ray absorption fine structure (EXAFS). The PL images and spectra of individual GeONWs were obtained with a confocal microscope. The origin of PL from GeONWs has been investigated by X-ray-excited optical luminescence (XEOL) spectroscopy using synchrotron radiation. XAFS and XEOL have been shown to be powerful tools for studying the electronic and optical properties of one-dimensional semiconductor nanomaterials.[12,13] XANES probes the unoccupied densities of states above the Fermi level through electric dipole transitions, and EXAFS provides information on the local structure including the interatomic distance and the local dynamics of the system. XEOL is an X-ray-photon-in, optical-photon-out technique that can provide site and excitation-channel specificity. The XEOL technique monitors the optical response of a light-emitting material by tuning the X-ray energy to a specific excitation channel (often at the X-ray absorption edge of an element of interest) and monitoring the luminescence with an optical monochromator (typically in the range of 200−900 nm). The relative quantum yield of the luminescence chromophore, which

Received: February 26, 2011
Revised: May 10, 2011
Published: May 20, 2011

is due to either excitons (the recombination of a hole in the valence band with an electron in the conduction band) or defects, depends strongly on the site and chemical environment of the absorbing atom.[14,15] Synchrotron-radiation-induced XEOL from GeONWs shows strong green light at 540 nm, which corresponds to the laser-excited photoluminescence. The strong emission is attributed to defects involving oxygen vacancies confirmed by XAFS and XEOL results.

EXPERIMENTAL SECTION

The GeONWs were prepared in a horizontal tube furnace system. High-purity Ge powder (99.999%, Alfa Aesar) was placed in the middle of the high-temperature zone of a quartz tube. Gold nanoparticles (20 nm) were dispersed as a catalyst on a Si(100) substrate for GeONW growth. The substrate was placed in the low-temperature zone (approximately one-fourth of the tube length from the end). When the tube was evacuated to a base pressure of 10^{-1} Torr prior to the growth, germanium oxide nanowires were obtained, whereas when the base pressure of the tube was controlled to 10^{-2}–10^{-3} Torr before the growth, pure Ge nanowires were obtained. The air remaining in the system was the oxygen source for GeONW growth. The carrier gas (Ar) was introduced from one end of the tube at 50 sccm (standard cubic centimeters per minute), and the system pressure was 200–400 Torr. The temperature of the furnace was increased to 930 °C at a rate of 15 °C/min and maintained for 1 h. The temperature of the nanowire growth zone was 475–580 °C as monitored by a thermocouple.

The morphology and structure of the as-synthesized products were characterized by SEM (FEI Quanta FRG 200F) and TEM (FEI Tecnai G2 F20 S-TIWN equipped with EDS, which provides the composition of the nanowires). The crystal structure of the as-synthesized products was obtained by XRD (D8 Focus), with Cu Kα radiation (λ = 1.5406 Å). The surface state and electron structure of the nanowires were obtained by XPS measurement [Kratos AXIS Ultra^{DLD} ultra-high-vacuum (UHV) surface analysis system], using Al Kα radiation (1486 eV) as a probe. An electron flood gun was used for all measurements to compensate charging, and the final spectra were calibrated to the adventitious carbon C 1s peak (284.6 eV). The PL images and spectra of individual GeONWs were obtained by confocal microscopy (Leica Tcs Sp5), and a 405-nm laser was used as the excitation source. X-ray absorption and XEOL experiments were conducted on the SGM beamline (250–1900 eV) at Canadian Light Source (CLS) for Ge L-edge and O K-edge measurements and on the BL14W beamline (4–29 keV) at Shanghai Synchrotron Radiation Facility (SSRF) for Ge K-edge measurements. The luminescence was monitored with a JY 100 monochromator equipped with a Hamamustu photomultiplier tube. All XEOL spectra were normalized to the incoming photon flux.

RESULTS AND DISCUSSION

Figure 1a shows an SEM image of the as-synthesized GeONWs on the Si substrate with high-yield nanowire growth. The diameter of the nanowires is in the range of 50–100 nm, and the length is up to tens of micrometers. The metallic catalyst nanoparticles are observed at the tips of the as-prepared GeONWs from the inset at the upper right of Figure 1a, providing direct evidence that the vapor–liquid–solid (VLS) mechanism is responsible for the GeONW growth. Figure 1b

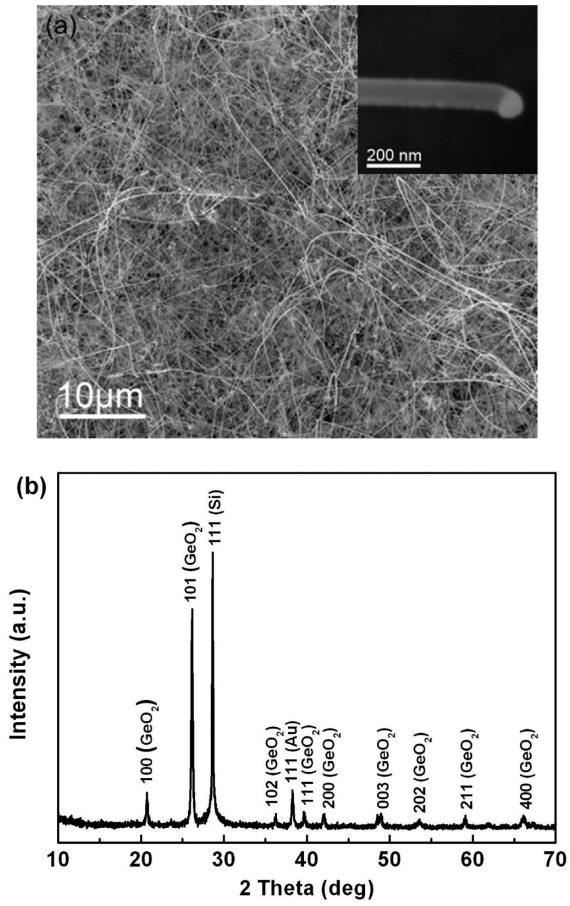

Figure 1. (a) SEM image of the as-synthesized nanowires. The inset at the upper right shows a single GeONW. (b) XRD spectrum of the as-synthesized GeONWs.

shows the XRD pattern of the GeONWs. The diffraction peaks can be attributed to quartz-like hexagonal GeO_2 (a = 4.99 Å, c = 5.65 Å, JCPDS no. 43-1016) and substrate Si. Figure 2a shows a representative TEM image of a single GeONW with a uniform diameter of about 100 nm along its entire length. The corresponding selected-area electron diffraction (SAED) pattern taken from the nanowire (shown in the upper-left inset in Figure 2a) reveals that the nanowire is a single crystal with a hexagonal structure. The high-resolution TEM (HRTEM) image (shown in the bottom-right inset in Figure 2a) further indicates that the as-prepared GeONWs are high-quality single crystals. The HRTEM image shows that the GeONW is structurally uniform and contains no noticeable defects such as dislocations and stacking faults. The interplane spacing of 0.34 nm corresponds to the d spacing of (101) crystal planes of hexagonal structure, and the growth direction of the nanowires is along [101]. Although crystalline GeO_2 is not stable under the high-density electron beam irradiation used during HRTEM imaging and easily changes to amorphous in a short time (around 20 s in our case), HRTEM images of GeONWs can be obtained by carefully taking the image quickly.[2,16] In a typical method to obtain an HRTEM image of the nanowires avoiding electron beam damage,[17] the focusing and crystal zone-axis orientation were performed on an adjacent region along the nanowire, and then the nanowire was moved to the area of interest, and the HRTEM image was quickly recorded. Both HRTEM and SAED

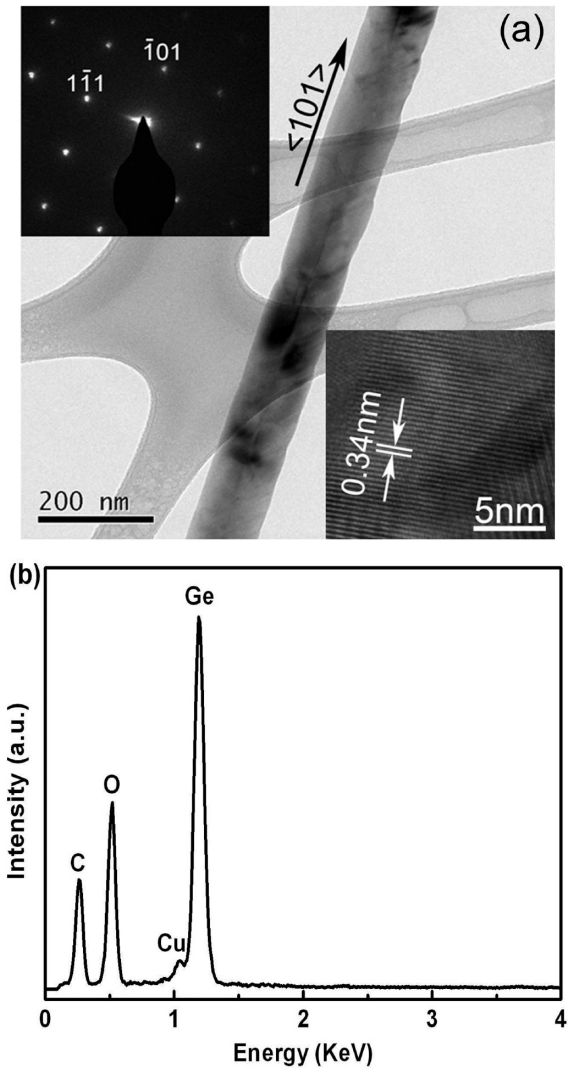

Figure 2. (a) TEM image of an individual as-synthesized GeONW. The inset at the upper left is the corresponding SAED pattern, and that at the lower right is an HRTEM image of the GeONW. (b) EDS spectrum of the GeONW in a.

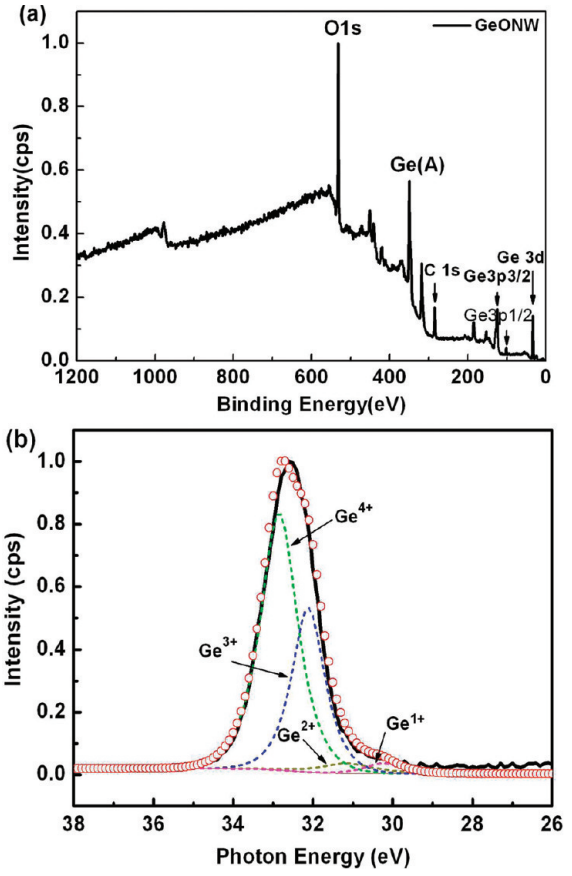

Figure 3. XPS spectrum of the GeONWs with peaks representing (a) the full spectrum and (b) the Ge 3d spectrum (black solid line). The red scatter circles and the continuous dotted lines for Ge^{+}, Ge^{2+}, Ge^{3+}, and Ge^{4+} are the fitted peaks.

results from individual nanowires and XRD analysis from all of the nanowires on average indicate that the GeONWs have a high-quality single-crystalline structure. The EDS analysis of an individual nanowire with a locally focused beam spot reveals (shown in Figure 2b) that the nanowires are composed of only germanium and oxygen with an atomic ratio close to 1:1.8. Thus, the chemical formula of the as-prepared nanowires is GeO_x ($x = 1.8$).

The electronic and chemical states of the GeONW surfaces were studied by XPS. Figure 3a shows the XPS full spectrum of GeONWs, which further confirms that the nanowires consist of only Ge and O. The C signal is from organic species absorbed on the GeONW surface. Figure 3b presents the Ge 3d electron state of the GeONWs. There is only one broad peak centered at 32.5 eV (black solid line) in Figure 3b, which is attributed to Ge 3d in germanium oxide. Schmeisser et al.[18] studied the Ge 3d spectra of oxidized Ge(100) and Ge(111) surfaces and isolated four surface oxidation states with a core-level shift of 0.85 eV per Ge−O bond or per oxidation state (Ge is octahedrally coordinated in the 4+ oxidation state with each O shared by two Ge atoms). The broad Ge 3d peak obtained from the GeONWs could be fit as a combination of four oxide peaks associated with the Ge^{+}, Ge^{2+}, Ge^{3+}, and Ge^{4+} oxidation states with energy states centered at 30.25, 31.1, 31.95, and 32.8 eV, respectively.[19] The peak area percentage of the Ge^{4+}, Ge^{3+}, Ge^{2+}, and Ge^{+} oxidation states are about 61.5%, 34.6%, 1.9%, and 1.9%, respectively, which corresponds to an atomic ratio of Ge to O of 1:1.8. This is consistent with the composition analysis from EDS and further confirms the oxygen deficiency in the GeNOWs. The main oxidation states of Ge in GeONWs are Ge^{4+} and Ge^{3+}.

The electronic structure and local structure of the GeONWs were also investigated by XAFS, which deals with the measurement and interpretation of absorption coefficients above a specific absorption edge, in this case, the Ge K-edge and $L_{3,2}$-edge. The excitations in the near-edge region in the vicinity of the threshold arise from the core-to-bound and -quasibound unoccupied-state dipole transitions. These features are reflected in the XANES analysis, which probes the densities of states and local symmetry. As the excitation energy increases, the photoelectron gains sufficient energy to leave the absorbing atom. As the photoelectron travels away from the absorbing atom, it will be scattered by the neighboring atoms. Therefore, the constructive and destructive interferences of these outgoing and backscattered waves produce oscillations in the absorption coefficient.

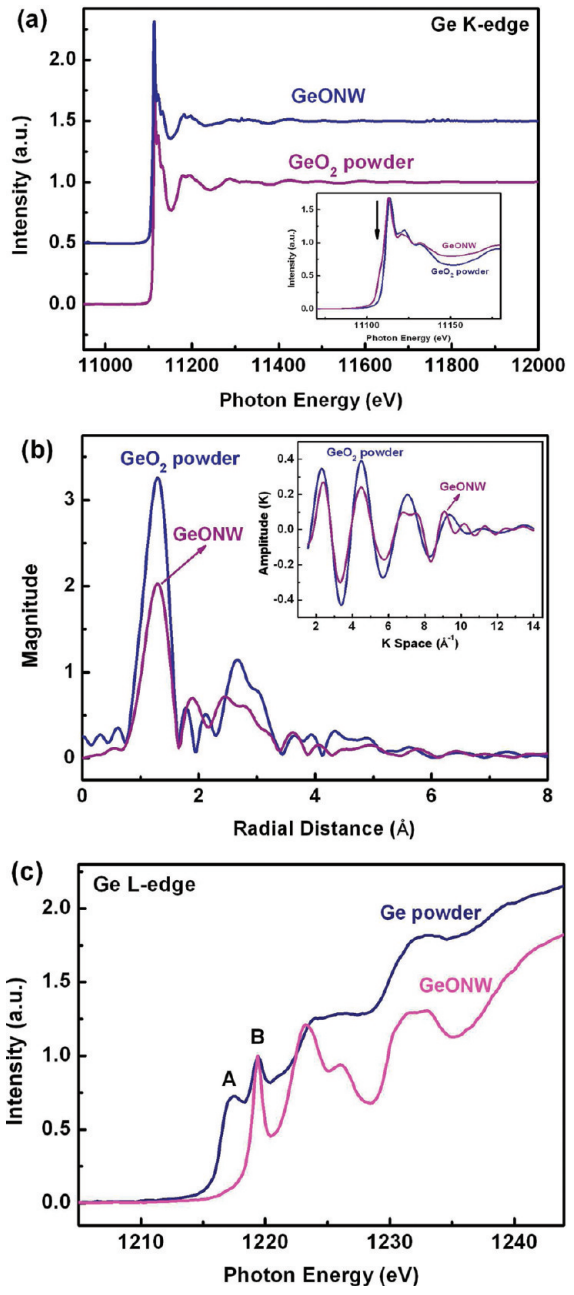

Figure 4. (a) Ge K-edge XAFS of GeONWs and GeO_2 powder; (b) Fourier transform EXAFS spectrum with k weighting, with an inset showing the filtered Fourier back-transform of the first shell for GeONWs and GeO_2 powder; and (c) Ge $L_{3,2}$-edge XANES of GeONWs and Ge powder.

These oscillations give rise to the EXAFS, denoted $\chi(k)$, which contains information about the interatomic distance and the local dynamics of the system, $\chi(k) = \phi(k)\,A(k)$, where $\phi(k)$ is the phase (containing bond-length and phase information) and $A(k)$ is the amplitude (containing information about the backscattered atom; the bond length; the coordination number; and the Debye−Waller factor, i.e., the thermal mean square displacement of the interatomic distance). EXAFS is sensitive only to short-range order because of the short attenuation length of electrons. EXAFS can be readily analyzed using a Fourier transform technique, which separates the phase and the amplitude. Figure 4a shows the Ge K-edge XAFS of the as-prepared GeONWs compared with GeO_2 crystalline powder of several micrometers in diameter with a quartz-like structure, which is regarded as bulk GeO_2. The inset displays the XANES region. Figure 4b shows the Fourier transform EXAFS spectrum with k weighting (data range: $k = 2-12$ Å for GeO_2 and GeONWs). One can see from the XAFS that the oscillation pattern for GeONWs resembles that of bulk GeO_2, indicating that they have essentially the same hexagonal lattice with a quartz-like structure. For GeONWs, the broadening of the oscillations of the sharp features observed in bulk GeO_2 is attributed to disorder such as a lack of coordination number (CN) and degradation of long-range order in the nanowires. The details are discussed later in this article. The Ge K-edge XANES analysis shows an interesting mismatch despite the similarity in the EXAFS data. A shoulder band can be seen before the edge jump (11110 eV) in the GeONWs, which is not seen in the GeO_2. The shoulder band arises from Ge with a low oxidation state (mainly Ge^{3+}), that is, the surplus Ge in the crystal lattice due to the substoichiometry of oxygen in the GeONWs. The Fourier transform EXAFS spectrum of the Ge K-edge in Figure 4b clearly shows the first- and second-shell Ge−O distance of the bulk GeO_2. The GeONW sample shows only one clearly identifiable peak at the first shell with nearly the same position and a noticeable reduction in amplitude. Table 1 lists the coordination number and interatomic distance of Ge−O in GeONWs obtained by fitting the Ge−O first-shell phase of GeONWs compared to bulk GeO_2. There is an obvious lack of coordination number in GeONWs (2.4 ± 0.2) compared to that of bulk GeO_2 (4.0), which is in good agreement with the XPS results and the fact of the oxygen deficiency in GeONWs. The Ge−O interatomic distance in the GeONWs is slightly longer than that in bulk GeO_2, which is mainly due to the weak Ge−O bonds in the environment of Ge with low oxidation states. The increase in Ge−O bonding length of a large amount of surface atoms at the nanowires owing to the nanosize effect probably also leads to a slight increase of the interatomic distance, on average. The amplitude reduction is attributed to the lack of long-range order due to the nanosize in one-dimension and the oxygen vacancy (lack of coordination number) in the GeONWs discussed above. This can be seen in the inset of Figure 4b, where the reduction in amplitude of the filtered Fourier back-transform of the first shell for GeONW relative to bulk GeO_2 is displayed. It should be noted that an amplitude reduction can be seen even in perfect nanosize single crystals; this is because the coordination number decreases at the surface and interface of the crystal, which also introduces chemical inhomogeniety. All of these effects are sometimes termed disorder. The Ge $L_{3,2}$-edge XANES data of GeONWs compared to Ge powder are shown in Figure 4c. The Ge $L_{3,2}$-edge XANES arise from the excitation of the 2p core-level electron into unoccupied states of 4s character above the Fermi level. The first resonance (marked A) at the Ge $L_{3,2}$-edge in Ge powder corresponds to the 2p-to-s transition from the unoxidized Ge, and the second resonance (marked B) is characteristic of Ge in an oxygen environment (GeO_2) from surface oxidation of Ge. In the GeONWs, the Ge $L_{3,2}$-edge exhibits an apparent GeO_2 sharp peak with a slight edge rising at position A that is due to Ge with low oxidation states consistent with the Ge K-edge.

The optical properties of GeONWs were studied by laser and synchrotron X-ray excitation. The PL of GeONWs can be easily monitored by confocal microscope and shows dynamic behavior under laser irradiation. Figure 5a shows a PL image of several

Table 1. Parameters for GeONWs Using FEFF[24] and IFEFFIT[25]

sample	shell	CN[a]	R^b (Å)	$\Delta\sigma^{2\,c}$ ($\times 10^{-3}$ Å)	ΔE_0 (eV)
GeO_2 (quartz)	Ge−O	4.0	1.73	–	–
GeONWs	Ge−O	2.4 ± 0.2	1.74 ± 0.02	1.07 ± 0.21	5.21 ± 0.52
GeONWs (annealed)	Ge−O	3.9 ± 0.4	1.74 ± 0.02	0.05 ± 0.10	7.75 ± 1.08

[a] Coordination number (CN). [b] Coordination distance. [c] Debye−Waller factor accounting for thermal and statistical vibration. Amplitude reduction factor (S_0^2) was fixed at 0.98. *R*-space fit: Δk = 2.0−12.0 Å, Δr = 0.8−2.0 Å, eight statistically justified free parameters.

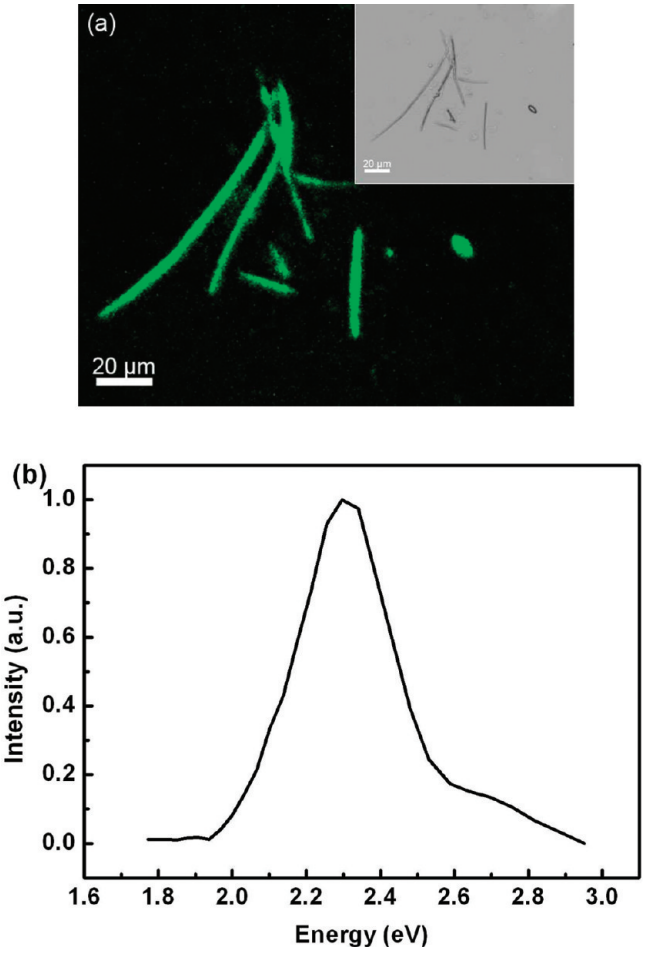

Figure 5. (a) PL image of several individual GeONWs. The inset at the upper right shows the optical bright-field image of the corresponding nanowires. (b) Typical PL spectrum of a selected single GeONW.

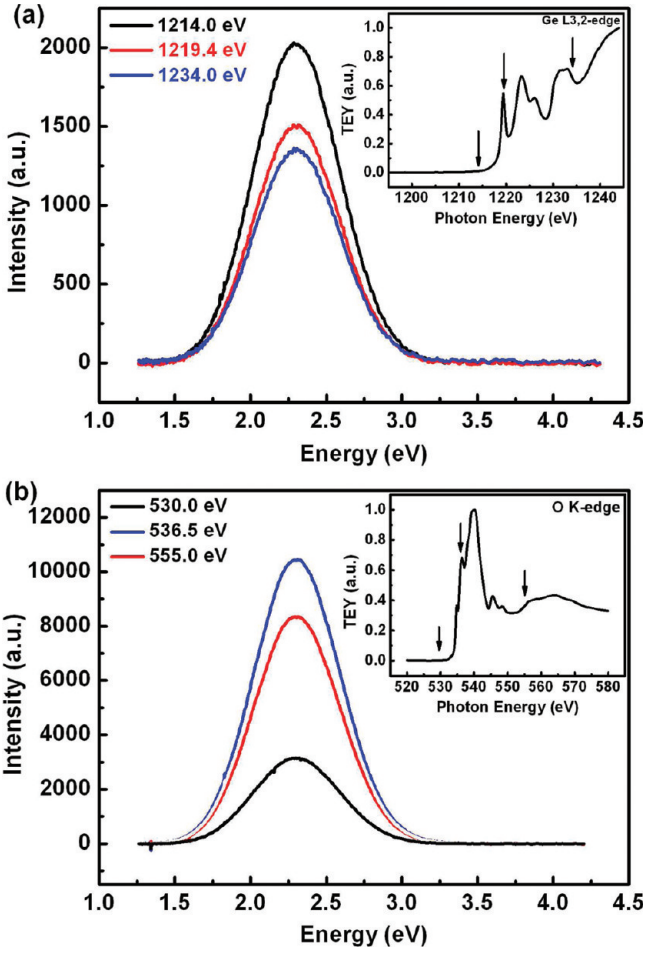

Figure 6. XEOL spectra of GeONWs excited across (a) the Ge L-edge, excited at the Ge L pre-edge (1214.0 eV), edge (1219.4 eV), and postedge (1234.0 eV), with an inset showing the XANES of Ge L-edge, and (b) the O K-edge, excited at the O K pre-edge (530 eV), edge (536.5 eV), and postedge (555 eV), with an inset showing the XANES of the O K-edge.

individual GeONWs dispersed on the Si substrate. The inset at the upper left is the corresponding optical bright-field image of the nanowires. The GeONWs emitted bright green light under a 405-nm self-contained argon-ion laser. A typical PL spectrum of a selected single GeONW is shown in Figure 5b. The broad PL peak ranges from 1.94 eV (640 nm) to 2.95 eV (420 nm) and is centered at 2.30 eV (540 nm). To investigate the origin of the PL of GeONWs, synchrotron-induced XEOL from GeONWs was obtained. Parts a and b of Figure 6 show the XEOL spectra of the GeONWs excited across the Ge L-edge and O K-edge, respectively. The insets of the Figure 6a,b are the XANES spectra of the Ge L-edge and O K-edge, respectively. XEOL of GeONWs excited at either the Ge L-edge or O K-edge energy range exhibits the same broad PL emission band centered at 2.3 eV (540 nm), corresponding to the PL spectrum of individual nanowires excited by a laser. When excited across the Ge L-edge, such as pre-edge (1214.0 eV), edge (1219.4 eV), and postedge (1234.0 eV), the GeONWs showed weak PL, and the emission intensity decreased with increasing excitation energy. However, when the GeONWs were excited at the O K pre-edge (530 eV), edge (536.5 eV), and postedge (555 eV), the emission intensity was much stronger than that excited at Ge L-edge. One also can see the strongest emission intensity at the O K-edge (536.5 eV), which is about 5 times stronger than that excited at the O K pre-edge, and then the PL is attenuated for O K postedge excitation. From these observations, one can immediately conclude that the strong green light emission at 2.3 eV peak is related to oxygen in the GeONWs.

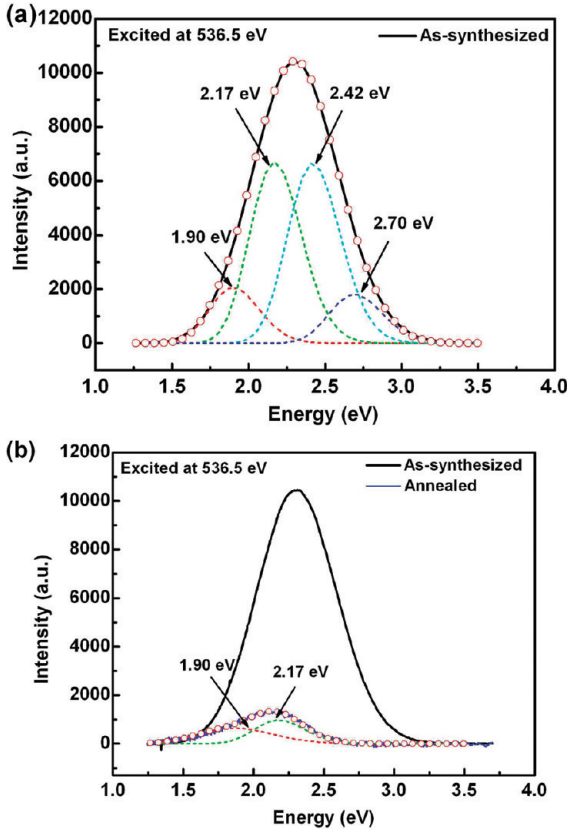

Figure 7. (a) XEOL of GeONWs excited at the O K-edge of 536.5 eV fitted by four components. (b) XEOL spectra of the GeONWs excited at the O K-edge (536.5 eV) before and after annealing. The XEOL of GeONWs after annealing is fitted by two Gaussian functions. The thick solid curve represents the experimental spectrum, and the dotted lines denote the entire fitted curve.

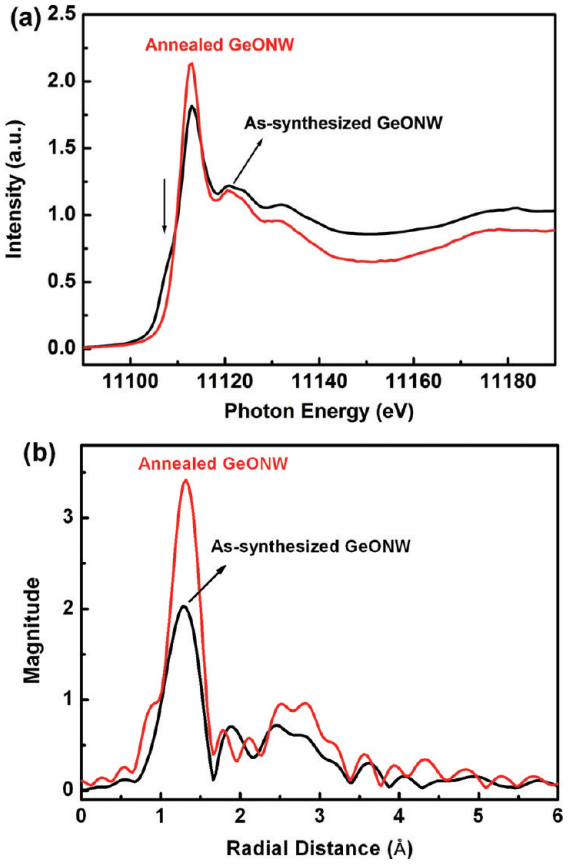

Figure 8. (a) Ge K-edge XANES of GeONWs before and after thermal annealing. (b) Fourier transform EXAFS spectrum with k weighting.

The XEOL spectra of GeONWs can be fitted with Gaussian functions in order to obtain insight into the photoluminescence of the GeONWs. The XEOL spectrum of the as-synthesized GeONWs excited at the O K-edge (536.5 eV) was fitted with four components (1.90, 2.17, 2.42, and 2.70 eV), which fit the experimental data very well (Figure 7a). The blue light emission (~2.7 eV) has previously been observed in Ge nanostructures.[8,9] The green PL (2.1−2.5 eV) of GeO_2 was reported in Ge crystals or Ge nanocrystals embedded in GeO_x ($0 < x < 2$) thin films.[20−22] Both blue and green light emissions are attributed to oxygen vacancies and germanium−oxygen vacancy centers.[8,9,20−22] The double oxygen vacancy is also deemed to be the most suitable target for generating bright blue photoluminescence for quartz-like GeO_2 nanowires.[10,11] Red light emission has been observed from glassy GeO_2,[23] which can be ascribed to nonbridging oxygen hole centers. In our case, the synchrotron-X-ray-induced PL intensity is sensitive only to the excitation energy at oxygen and independent of that at Ge. Based on the fact that there is an oxygen deficiency in GeONWs, the strong green PL from GeONWs can be further attributed to defect states in the band gap arising from the oxygen involved in the vacancy centers. We found that there is no obvious change in the area ratios of the four components with the various excitation energies from Ge $L_{3,2}$-edge to O K-edge. Because all four components arise from oxygen-related defects, X-ray excitation cannot distinguish among the different defect states.

To confirm that the PL of GeONWs comes from oxygen deficiencies, thermal annealing of the as-synthesized GeONWs was performed to remove the oxygen vacancies in the GeONWs. The as-synthesized GeONW sample was annealed in air at 450−500 °C for 1 h. Figure 7b shows the XEOL spectra of the GeONWs excited at O K-edge (536.5 eV) before and after annealing. The XEOL spectrum of annealed GeONWs exhibits a much more attenuated PL emission compared with that of as-synthesized GeONWs. The best fit of the annealed GeONWs was obtained with only two peaks centered at 1.90 and 2.17 eV (Figure 7b). In addition to the significant decrease of the intensity of XEOL, the blue and blue-green emission bands (2.70 and 2.42 eV) disappeared after annealing because of the removal of most of the oxygen vacancies in the GeONWs. Figure 8a shows the Ge K-edge XANES spectrum of the annealed GeONWs compared to that of the as-synthesized GeONWs. Figure 8b shows the EXAFS Fourier transform spectrum with k weighting (data range: $k = 2-12$ Å). After thermal annealing, the shoulder band in the XANES spectrum of as-synthesized GeONWs arising from the Ge with low oxidation state (mainly Ge^{3+}) disappears in that of annealed GeONWs. The XANES spectrum of annealed GeONWs shows a feature similar to that of bulk crystalline GeO_2. The Fourier transform of the Ge K-edge EXAFS spectrum of annealed GeONWs in Figure 8b clearly shows the first and second shells Ge−O distances, similar to those in the bulk GeO_2 and with a restored amplitude compared to that in as-synthesized GeONWs. The coordination number in annealed GeONWs changes to 3.9 from 2.4 in as-synthesized

GeONWs, which approaches that of bulk GeO_2 (4.0). All of these results confirm that the as-synthesized GeONWs were further oxidized to GeO_2 nanowires with far fewer oxygen vacancies by thermal annealing in the air.

CONCLUSIONS

In summary, high-quality single-crystalline germanium oxide nanowires with diameters varying from 50 to 100 nm and lengths of up to tens of micrometers have been synthesized by a thermal evaporation method under a VLS mechanism. The electronic structure and local structure of the GeONWs were also investigated by XAFS. The XAFS results show disorder and degradation of long-range order in the nanowires because of the nanosize in one dimension and the oxygen vacancies in the nanowires. Synchrotron-radiation-based XEOL spectroscopy from GeONWs shows strong green light at 540 nm, which corresponding to the PL spectrum of selected single germanium oxide nanowires. The strong green emission is attributed to oxygen-related defect states arising from an oxygen deficiency, as confirmed by XEOL combined with XANES.

AUTHOR INFORMATION

Corresponding Author

*E-mail: xhsun@suda.edu.cn (X.S.), jiangzheng@sinap.ac.cn (Z.J.).

ACKNOWLEDGMENT

The authors thank Xiaoqing He (TEM) and Xiaoye Chen (XPS) for experimental support. The authors also thank beamline BL14W (Shanghai Synchrotron Radiation Facility) for providing the beam time. Research described in this article was performed in part at the Canadian Light Source, which is supported by the Natural Sciences and Engineering Research Council of Canada, the National Research Council Canada, the Canadian Institutes of Health Research, the Province of Saskatchewan, Western Economic Diversification Canada, and the University of Saskatchewan. The work was supported by the National Basic Research Program of China (973 Program) (Grant 2010CB934500), Natural Science Foundation of China (NSFC) (Grant 51072127), and the Priority Academic Program Development of Jiangsu Higher Education Institutions.

REFERENCES

(1) Hidalgo, P.; Méndez, B.; Piqueras, J. *Nanotechnology* **2007**, *18*, 155203.
(2) Pei, L. Z.; Zhao, H. S.; Tan, W.; Zhang, Q. F *J. Appl. Phys.* **2009**, *105*, 054313.
(3) Yan, C. Y; Chan, M. Y.; Zhang, Z.; Lee, P. S. *J. Phys. Chem. C* **2009**, *113*, 1705–1708.
(4) Lin, Z. Y.; Garside, B. K. *Appl. Opt.* **1982**, *21*, 4324.
(5) Bai, Z. G.; Yu, D. P.; Zhang, H. Z.; Ding, Y.; Wang, Y. P.; Cai, X. Z.; Hang, Q. L.; Xiong, C. C.; Feng, S. Q. *Chem. Phys. Lett.* **1999**, *303*, 311.
(6) Hidalgo, P.; Méndez, B.; Piqueras, J. *Nanotechnology* **2005**, *16*, 2521.
(7) Hidalgo, P.; Liberti, E.; Rodríguez-Lazcano, Y.; Méndez, B.; Piqueras, J. *J. Phys. Chem. C* **2009**, *113*, 17200–17205.
(8) Zacharias, M.; Fauchet, P. M. *J. Non-Cryst. Solids* **1998**, *227*, 1058.
(9) Wu, X. C.; Song, W. H.; Zhao, B.; Sun, Y. P.; Du, J. J. *Chem. Phys. Lett.* **2001**, *349*, 210–214.
(10) Zyubin, A. S.; Mebel, A. M.; Lin, S. H. *J Phys. Chem. A* **2007**, *111*, 9479–9485.
(11) Zyubin, A. S.; Mebel, A. M.; Lin, S. H. *J. Chem. Phys.* **2006**, *125*, 064701.
(12) Zhou, X. T.; Kim, P. S. G.; Sham, T. K.; Lee, S. T. *J. Appl. Phys.* **2005**, *98*, 24312.
(13) Sun, X. H.; Lam, S.; Sham, T. K.; Heigl, F.; Jurgensen, A.; Wong, N. B. *J. Phys. Chem. B* **2005**, *109*, 3120–3125.
(14) Sham, T. K.; Naftel, S. J.; Kim, P. S. G.; Sammynaiken, R.; Tang, Y. H.; Coulthard, I.; Moewes, A.; Freeland, J. W.; Hu, Y. F.; Lee, S. T. *Phys. Rev. B* **2004**, *70*, 045313.
(15) Sun, X. H.; Wong, N. B.; Li, C. P.; Lee, S. T.; Sham, T. K. *J. Appl. Phys.* **2004**, *96*, 3447–3451.
(16) Zhang, Y. J.; Zhu, J.; Zhang, Q.; Yan, Y. J.; Wang, N. L.; Zhang, X. Z. *Chem. Phys. Lett.* **2000**, *317*, 504–509.
(17) Bell, D. C.; Wu, Y.; Barrelet, C. J.; Gradecak, S.; Xiang, J.; Timko, B. P.; Lieber, C. M. *Microsc. Res. Tech.* **2004**, *64*, 373–389.
(18) Schmeisser, D.; Schnell, R. D.; Bogen, A.; Himpsel, F. J.; Rieger, D.; Landgren, G.; Morar, J. F. *Surf. Sci.* **1986**, *172*, 455–465.
(19) Hanrath, T.; Korgel, B. A. *J. Am. Chem. Soc.* **2004**, *126*, 15466–15472.
(20) Palm, J.; Gan., F.; Zheng, B.; Michel, J.; Kimerling, L. C. *Phys. Rev. B* **1996**, *54*, 17603.
(21) Kartopu, G.; Bayliss, S. C.; Hummel, R. E.; Ekinci, Y. *J. Appl. Phys.* **2004**, *95*, 3466.
(22) Oku, T.; Nakayama, T.; Kuno, M.; Nozue, Y.; Wallenberg, L. R.; Niihara, K.; Suganuma, K. *Mater. Sci. Eng. B* **2000**, *74*, 242.
(23) Skuja, L.; Hosono, H.; Mizuguchi, M.; Güttler, B.; Silin, A. *J. Lumin.* **2000**, *87−89*, 699–701.
(24) Zabinsky, S. I.; Rehr, J. J.; Ankudinov, A.; Albers, R. C.; Eller, M. J. *Phys. Rev. B* **1995**, *52*, 2995–3009.
(25) Newville, M. *J. Synchrotron Radiat.* **2001**, *8*, 322–324.